ISME

Iranian Journal of Mechanical Engineering
The Iranian Society of Mechanical Engineers
Research Paper

DOI: 10.30506/JMEE.2022.524861.1253

Residual Stress Assessment in Spiral Steel Pipe with the Grade of API-X65 after Submerged Arc-welding

M. Rajabi[*]
Ph.D.

SH. Hashemi[†]
Professor

In this study, residual stresses in a finite sample separated from the seam-weld of an API pipe with a large diameter were studied for the first time. A finite element simulation of the welding process was conducted to achieve a safe dimension for this sample. After validation of the results, residual stresses were obtained in different directions in this way. Residual stress distribution in the thickness direction represented for the first time is important; firstly, based on standards the accuracy of central-hole-drilling results depends on it. Secondly, this distribution sheds light on the 3D equilibrium of residual stresses. The results show that a finite sample with the size of 320×440 mm separated from the main pipe is appropriate for doing the central-hole-drilling test which is a significant achievement. It is also proved that the maximum value of residual stresses takes place on surfaces of the sample, while the minimum of this figure was reported in the middle of the thickness. This achievement ensures that the maximum and critical values of residual stresses are obtained by the CHD technique.

Key Words: Residual stress, Spiral welded pipe, Hole drilling technique, Natural gas transmission pipes, API X65

1 Introduction

The residual stress (RS) is a kind of stress which remains in a solid body after the elimination of external loads. It can be created due to plastic deformation, temperature gradient or deformation in the structure, etc. For instance, the heat produced through the welding process leads to local thermal expansion in the body. The body may reach the ambient temperature after welding and rapidly become concave resulting in local RS [1]. Generally, API pipes are used with large diameters and withstand high internal pressures. Welding RS reduces design or working stress in large diameter and high-pressure natural gas transportation pipes. Although in recent decades there have been done plenty of works to understand the residual stress and even finding ways to reduce its values and improve welded materials' strength, the industry still requires promoting the mechanical properties of the weld with RS. Therefore, more studies are demanded in this area. Majzoobi et al. determined RS in the ST-37 steel plate with the dimension of 12.5×180×130 mm that was welded

* Corresponding Author, Ph.D., Pipes and Related Industries Research Center, University of Birjand, Birjand, Iran P.O.B. 97175/615, Mohamad_rajabi@birjand.ac.ir

† Professor, Department of Mechanical Engineering, University of Birjand, Birjand, Iran, P.O.B. 97175/615, shhashemi@birjand.ac.ir

Receive: 2021/02/09 Accepted: 2022/03/13

through arc welding [2]. Accordingly, finite element simulation (FE) was done, the temperature distribution was presented, and the FE and experimental results were compared. Results demonstrate that the mechanical properties of a material are dependent on the temperature of the structure and Such a relationship is important to study. Moreover, the effect of different parameters such as travel welding, fixture, material behavior, thickness, and the number of welding passes is studied on RS in the welding region. Sattari-Far et al. determined RS in the weld seam of stainless steel pipe of the grade AISI-304 by FE and central hole drilling (CHD) technique which is a renowned and affordable technique to determine residual stresses in Iran because of high expenses and lack of modern facilities. The pipe diameter was 320 mm and the wall thickness was 10 mm and also welding was done using the tungsten inert gas (TIG) technique. RS depends on groove weld geometry and the number of welding passes. By increasing the number of passes, the value circumferential RS in the center of the weld seam increases while longitudinal RS declines [3]. Forouzan et al. determined RS in the weld seam on API X70 spiral steel pipe with the outside diameter of 1,219.2 mm and a wall thickness of 20.6 mm welded through submerged arc welding (SAW). In the recent study, FE simulations and laboratory tests were done. Hydrostatic test (HT) reduces tensile RS which was modeled in two steps. Firstly, the welding process of the pipe was modeled then a hydrostatic test was applied through analysis. Six strain rosettes were installed on the external surface and six strain rosettes were installed on the internal surface of the pipe at a distance of every ten millimeters. CHD test was done before and after the hydrostatic test and results were compared with the FE results. Because of high values of residual stresses before the hydrostatic test, the results of CHD have considerable errors [4]. Habibi et al. studied the welding process of an offshore structure both by simulation and experiments. The simulation data depicts that the heat-affected zone (HAZ) is developed in the entire thickness of the brace at the weld toe spot and about half the chord thickness. They have experimentally analyzed the fatigue life for the welded tubular X-joints of these offshore installations. Also, they investigated the influence of shot-peening on the fatigue life of some joints. The outcomes of the experiment indicate that the fatigue life of the shot-peened tubular joint is approximately twice that of the original tubular joint [5]. Farrahi et al. investigated the impact of repair on the fatigue life of tubular joints. That repair for the original samples improves the fatigue life by approximately 150 percent. The increase of fatigue life for shot-peened and repaired specimens is around 105 percent. Before and after fatigue loading, the in-depth residual stresses are estimated on the repaired joints. Generally, the repair made a remarkable refinement on the fatigue manners of studied tubular joints. Nevertheless, if repair is not possible, shot peening can be a good choice to enhance the fatigue life of welded joints. On the other hand, shot peening may not be financially or technically tenable if repair is planned [6]. Habibi et al. scrutinized the heat transfer and the corresponding residual stress for a three-stage arc welding procedure in an X-tubular joint made out of St52 employing Simufact Welding software. The FE includes the thermal and mechanical properties of base and welding metals as a function of temperature. They used mesh adaptation during the process and meshing consistent with the welding area, the birth, and death method, and the source of heat transfer. Comparison of the outcomes indicates that the numerical data and experimental results are in proper accordance with each other, and the model can provide a fine foretelling for temperature and stress field control in this welding process [7]. Residual stresses have a hidden character because they exist locked in within a material [8]. Nakhodchi et al. evaluated temperature distribution and RS produced by multi-pass welding on AISI 321 stainless steel. The welding process was done by shielded metal arc welding (SMAW) and gas tungsten arc welding (GTAW). Samples with a dimension of 200×200 mm, wall thickness of 6 and 10 mm were used. Welding was done for different wall thicknesses of the model then was simulated by FE. The generated model is convenient for the

assessment of the welding process [9]. In another work, circumferential welding of API X70 pipe with a diameter of 1,423 mm and a wall thickness of 19.8 mm was studied. CHD technique was performed on both external and internal sides of the pipe. Maximum compressional stress in the circumferential and longitudinal directions, both on the internal and external sides of the pipe, occurs at a distance of 30 mm from the weld seam [10]. Charkhi et al. studied the effect of preheating on the reduction of RS on A106-B Carbone steel pipe with a diameter of 1,023 mm and a wall thickness of 5.8 mm. Reported tensile stresses, on both internal and external sides of the pipe in the longitudinal direction, were decreased with the promotion of preheating temperature [11]. Results of another study show that by changing the joint geometry from V-groove to X-groove, the maximum values of RS, as well as distortion, can be reduced by 20% and 15% respectively [12]. The effect of through-thickness RS on the stress intensity factor for a semi-elliptical surface crack in the Q345qD steel plate was investigated by Qiang et al. It was reported that longitudinal RS in the thickness direction caused the stress intensity factor on the crack tip to increase [13]. By modeling the process of welding according to the analysis of posterior thermal-mechanical stress, Haohui Xin et al. recently analyzed a specimen with compact tension. Using the residual stress distribution caused by welding, which is numerically predicted, they investigated the residual stress effects on the fatigue crack growth rate. Then, a comparison is presented between the fatigue crack growth rate considering the residual stress effects of parent material with the HAZ and the welds [14]. Furthermore, the residual stress in the thickness direction is investigated systematically by electron backscatter diffraction and neutron diffraction. Based on the results of the new study, along the thickness direction, the residual stresses of macroscopic and macroscopic plus elastic mismatch are decreased [15]. In another recent work, S. Goel et al. measured residual stresses in PBF built alloy 718 by neutron diffraction. Then, they studied the thermal post-treatments and process parameters effects on RS. According to their results, residual stresses are effectively reduced by thermal post-treatment. Moreover, it was shown that laser-based PBF built material had a higher RS in comparison with electron-beam-based PBF built material [16]. Moreover, the RS of the hoop structure made by cooling shrinkage of the weld was investigated when the outer cylinder was wrapped before welding and when the inner cylinder exists. The results of this study suggest that with the increase of the welding energy, the width of the weld seam, the radius of the container, the welding speed, and the thickness of the laminate, the value of maximum RS in the outer plate surface of the hoop structure decreases [17]. Magnier et al. applied the scope of the CHD technique to thin plates. In their work, the CHD technique was applied on an austenitic-ferritic brazed sheet metal construction [18]. In another study, moreover, the effects of thickness on the CHD results by FE were examined. A method is introduced to analyze the RS in plates with an intermediate thickness. The method is appropriate to specify a general in-depth non-uniform RS distribution [19]. An experimental study was conducted using the hole-drilling and sectioning methods to examine and model the RS in normal strength steel and high-strength steel with 45 specimens. With an increase in the steel strength, the ratio of maximum compressive RS gradually decreased. Nonetheless, the variation in the tensile RS in the vicinity of the weld seam in the middle section was not affected by varying the parameters altered during the experiment that are diameter-to-thickness ratio, the processing techniques, steel strengths, and welding locations. In contrast with those of welded approach, in the hot-rolled seamless circular steel tube sections, the RS along the circumferential direction of the inner or outer surfaces were approximately identical, which is in agreement with the theoretical model of the ECCS [20]. However, it would be highly valuable if the experimental results were compared with results of finite element simulations of the experiences after which the probable differences would be discussed. Through thickness, RS is important because the validation of the CHD technique

depends on it. Variation of RS in the thickness direction should be small to do CHD technique and maximum RS should also be less than half of the yield strength of material [21]. Experimental measurement of RS and also FE are playing an important role in finding RS in the welded pipes. In our work, all the aforementioned points are observed. Furthermore, through-thickness RS which is obtained by FE for API X65 pipe is reported for the first time in this paper. Since transportation of these pipes is difficult due to their heavyweight and large dimensions, separating a standard sample would be an easier choice to determine RS by CHD technique. According to the results of a previous study, the initial dimensions of the finite sample are considered 320×440 mm. Consequently, finite element simulation should be done to ensure that residual stresses at the center point of this sample are similar to that of an intact pipe [22].

Commercial software packages like ABAQUS [23] have been increasingly used to investigate diverse welding techniques [24-27]. This software has the ability for combined thermal-mechanical analysis via user subroutines. Deshpande et al. proved that the expected thermal histories, RS and strains, and stress relaxation during post-weld heat treatment by SYSWELD and ABAQUS were in satisfactory agreement [28]. Michaleris et al. employed ABAQUS to foresee welding-induced distortion and to evaluate the structural integrity of immense and complicated structures. They embraced a decoupled thermal-mechanical computation procedure, in which the welding-induced RS was obtained employing a 2D FE model for structural study. Fricke et al. scrutinized the RS induced by welding shrinkage during a multi-pass pipe girth welding [25] utilizing a complete 3D FEM. Dong et al. [26] likewise studied the RS in a multi-pass girth welded stainless steel pipe employing ABAQUS. They made FEM using shell elements, and the weld metal process was modeled operating the ABAQUS User Subroutine (UMAT). Zhang et al. utilized the shell element FEM and ABAQUS/UMAT method [27] to investigate the 3D RS in pipe restoration welds. The influence of repair length on RS was also studied.

In this study, after validation of the results, this finite sample is used to determine RS in longitudinal, circumferential, and thickness directions for API X65. Finally, the results are compared to that of the CHD technique determined at the mid-points on both surfaces of the sample.

2 Characteristics of API X65 spiral steel pipe

API steel pipes are low Carbone and low alloy steels. During the production process of spiral pipes, a steel sheet enters the forming machine and is formed spirally proportionate to the desired outside diameter [29]. SAW is a dominant welding method for these spiral steel pipes. This welding technique yields high RS in the welding region [4]. Submerged arc welding with a high sedimentation rate is firstly done on the internal side and then on the external side of the spiral pipe with two or three weld torches, then the pipe is sliced to the required length. According to API standard, the outside diameter of spiral pipes is between 508 mm and 2,000 mm, and these pipes are produced with a thickness from 6 to 20 mm and also with a length between 8 and 18 m.

2.1 Definition of stress coordinate for spiral-pipes

Figure (1) shows the main directions of RS in the weld-line of a spiral pipe under internal pressure. σL is longitudinal stress, σ_H is hoop stress, σ_N is normal stress and σ_T is tangential stress, applied to the WS. Normal stress exerted on WS is divided into longitudinal and hoop stresses in the spiral pipes, so WS of these pipes withstands lower direct stress rather than longitudinal welded pipes [21].

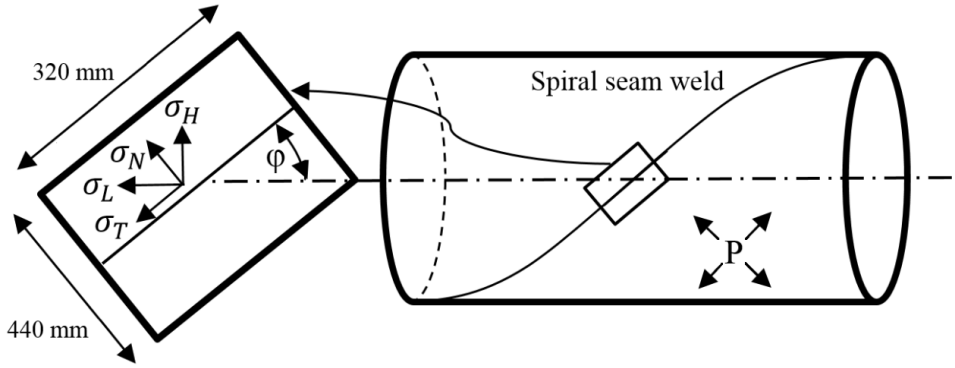

Figure 1 Direction of stresses on the sample containing WS of spiral-pipes [17]

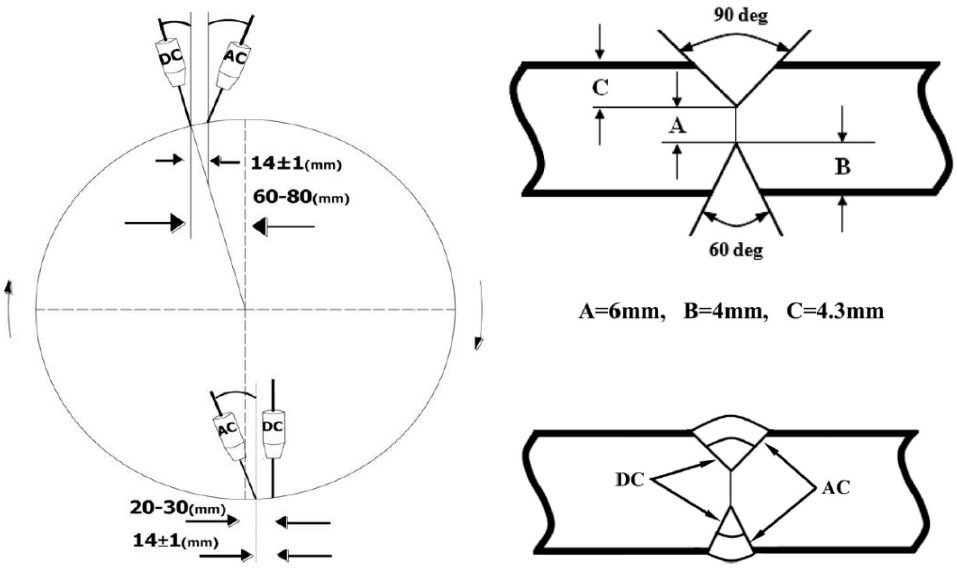

Figure 2 The geometry of groove weld and welding torch arrangement for spiral WS of API-X65 pipe [30]

It was shown that RS numbers converge to zero at the distance of 320×440 mm from a point located on the WS [4]. Because the dimension of the sample is much smaller than the diameter of pipe, a flat sample can be simulated. Dimension and location of the selected sample are shown in Figure (1). The sample is selected in a way that WS to be located in the center of the sample.
The geometry of WS for API-X65 steel pipe and also the location of welding torches for internal and external weld passes are shown in figure 2 [21].

2.2 Welding conditions for API-X65 pipe

API-X65 pipe is welded in a way that two passes are located on the internal side and two passes are located on the external side of the pipe. During the welding process, the weld pool is protected by a layer of preserving slag [30, 31]; This coating preserves the weld pool from contamination and concentrates welding heat into the weld pool and also oxides and cleans weld metal region (WM). The internal and external sides of the pipe are welded consecutively. Distance between subsequent passes in each side of the model is 14 mm and the distance between the internal and external passes is 2,370 mm, after dividing this value by welding travel speed, welding time between internal and external passes is obtained 119 seconds.

Table 1 Mechanical properties of API-X65 pipeline steel in different temperatures [30]

Temperature (K)	Yield stress (MPa)	Expansion (10^{-6} K) ratio	Poison ratio	Shear modulus (10^{4} MPa)	Young's modulus (GPa)	Specific heat (10^{6} J/m^3.K)	Thermal conductivity (W/m.K)
298	500	12.5	0.29	94.5	206	31.9	60.0
323	490	12.7	0.30	93.5	204	32.1	59.5
373	465	13.0	0.31	90.0	203	32.7	58.8
473	428	13.5	0.32	81.0	198	33.8	55.4
573	385	13.2	0.33	69.0	191	34.8	50.5
673	335	13.4	0.34	37.5	180	36.0	45.9
773	260	13.5	0.35	18.5	167	37.2	41.2
973	170	13.9	0.37	9.0	53	41.8	33.3
1173	105	11.0	0.39	4.0	25	35.4	28.5
1373	19	13.0	0.40	1	13	36.0	30.2
1573	6	14.5	0.44	-	2	36.5	32.1
1773	-	17.8	0.48	-	1	38.3	36.6
2023	-	-	0.48	-	-	39.2	39.9

2-3- Mechanical properties of API-X65 steel

Mechanical properties of API-X65 are required to simulate the welding process and are presented in table (1) as a function of temperature; Linear interpolation is used for other temperatures [32]. The yield strength of API-X65 pipeline steel at ambient temperature is 500 MPa.

3 Thermal loading

3.1 Heat transfer in the welding process

The heat is usually dissipated from the weld region by convection and radiation heat transfer [33]. The cooling time between the welding passes is both considered in reference [4] and the current study. The effect of radiation is considered as equivalent conduction coefficient which is:

$$h_{eq} = h_c + h_r = \begin{cases} 0.0668\theta & \mathrm{Wm^{-2}{}^oC^{-1}} \quad 0 \le \theta \le 500℃ \\ 0.231\theta - 82.1 & \mathrm{Wm^{-2}{}^oC^{-1}} \quad \theta > 500℃ \end{cases} \tag{1}$$

Where h_r and h_c are related to radiation and conduction and θ is the temperature (℃). The thermal energy distribution is an important factor required for thermal analysis of welding. The weld pool and HAZ size, cooling rate, and temperature gradient depend on these two parameters. Heat energy which is entered into the weld pool with electrical arc can be obtained as the following:

$$Q = \eta . V . I \tag{2}$$

Where V voltage, I is electrical current and η is the rate of efficiency of electrical arc. Table (2) shows the welding parameters. The rate of efficiency for ordinary submerged arc welding is usually more than 90% and it is considered 95% in the following analysis [32].

Table 2 Welding parameters for API-X65 pipe [32]

Pipe diameter (mm)	Welding pass	Number of welding torches	Type of welding torch	diameter of welding torch (mm)	Type of electrical current	Electrical current (*A*)	Voltage (*V*)	Welding speed (mm/minute)
1,219×14.3	Internal pass	1	S2MO	$\frac{16}{5}$	DC	700	31	$\frac{6}{5}$
	Internal pass	2	S2MO	$\frac{16}{5}$	AC	700	33	$\frac{6}{5}$
	external pass	1	S2MO	$\frac{16}{5}$	DC	800	31	$\frac{6}{5}$
	external pass	2	S2MO	$\frac{16}{5}$	AC	800	33	$\frac{6}{5}$

3.2 Goldak's heat source model

A mathematical model for surface and volume heat flux that is entered into the weld region is the Goldak double ellipsoid heat source [33]. This model is composed of two half of different ellipsoids that one of them is located in front of the heat region and the other is located in the back of the heat region. Figure (3) shows the Goldak model, as well as the hatched region, which shows one-dimensional heat flux. Moreover, *a*, *b*, *Cf*, *Cr* are constants of the Goldak model. These constants should be adjusted in a way that the two important parts of the weld region, WM, and HAZ, can be shown.

Where:

$$\begin{aligned} x_G &= x \\ y_G &= y \\ z_G &= z = vt \end{aligned} \tag{3}$$

v is based on welding travel speed, *x*, *y* and *z* are distances from a desired point in the coordinate system. x_G, y_G, and z_G are the distances from an arbitrary point in the mobile coordinate system (C_G) and are known as Goldak distances. The following equations show heat distribution in the front and back ellipsoids of the model:

$$q_f(x,y,z) = \frac{6\sqrt{3}f_f Q}{abc_f\pi\sqrt{\pi}} e^{\left(-\frac{3x^2}{a^2}\right)} e^{\left(-\frac{3y^2}{b^2}\right)} e^{\left(-\frac{3z^2}{c_f^2}\right)} \tag{4}$$

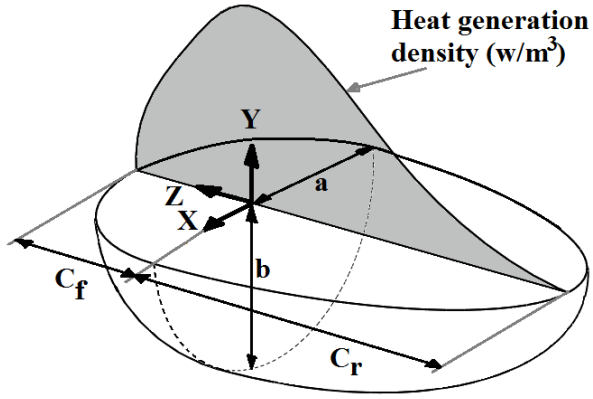

Figure 3 Goldak double ellipsoid heat source

$$q_r(x,y,z) = \frac{6\sqrt{3}f_r Q}{abc_r\pi\sqrt{\pi}} e^{\left(-\frac{3x^2}{a^2}\right)} e^{\left(-\frac{3y^2}{b^2}\right)} e^{\left(-\frac{3z^2}{c_r^2}\right)} \quad (5)$$

f_f and f_r are thermal parameters in the front and back regions of the model and are defined as follows:

$$f_f + f_r = 2 \quad (6)$$

$$f_f = \frac{2c_f}{c_f + c_r} \quad (7)$$

$$f_r = \frac{2c_r}{c_f + c_r} \quad (8)$$

Goldak model is used for optimization and assessment of heat entering the weld region. Moreover, *the element birth and death technique* is used for modeling the welding processes. Firstly, all elements of the body are modeled, then by a reduction ratio, the hardness coefficient of these elements is made so small and time out elements are made inactive; consequently, the mass and energy of dead elements are made inactive, too. Dead elements are made active as soon as the arrival of heat source. Meanwhile, the mechanical properties of a material are dependent on the temperature, as a result, yield strength and other material properties will be defined in the model as a function of temperature [34].

4 Finite element simulation of the sample

FE simulation of the sample is done by Abaqus software (the preferred software in this field) to determine RS in the thickness direction. Microstructure properties of API-X70 are defined as software based on the existing data [35]. The temperature of the material is high for a short limitation of time so it is assumed that creeping does not occur in the material. Meshing style is very important in the WS region. Stress and temperature gradient are high in the vicinity of the weld region, so small meshes should be used near the WS. The accuracy of the results is directly dependent on the number of elements, therefore sensitivity analysis of meshes is done. Elements are of C3D8T type that is thermal-displacement and 8-node couple.

Figure (4) shows the maximum temperature in the WS region during the welding process per number of elements. By comparing 40,000 elements to 30,000 elements, (1,958oC to 1,950oC) temperature variation is lower than 0.4%, so 40,000 elements with 100,500 meshes are used for simulation of the model.

Figure (5) shows the meshes of the sample. The relative length of the meshes in the vicinity of the sample is 1 mm. Weld cap was considered in the modeling process in this research, which was eliminated in reference [4] for simplification purposes both in simulation and for CHD analysis.

Latent heat required for phase change of liquid is considered by the conception of enthalpy. The coefficient of convection heat transfer is constant at 18°C on all surfaces of the sample during the welding process with the ratio of 15W/m^{2}K. The welding torch is located in the middle of each pass, 8 seconds after welding initiation.

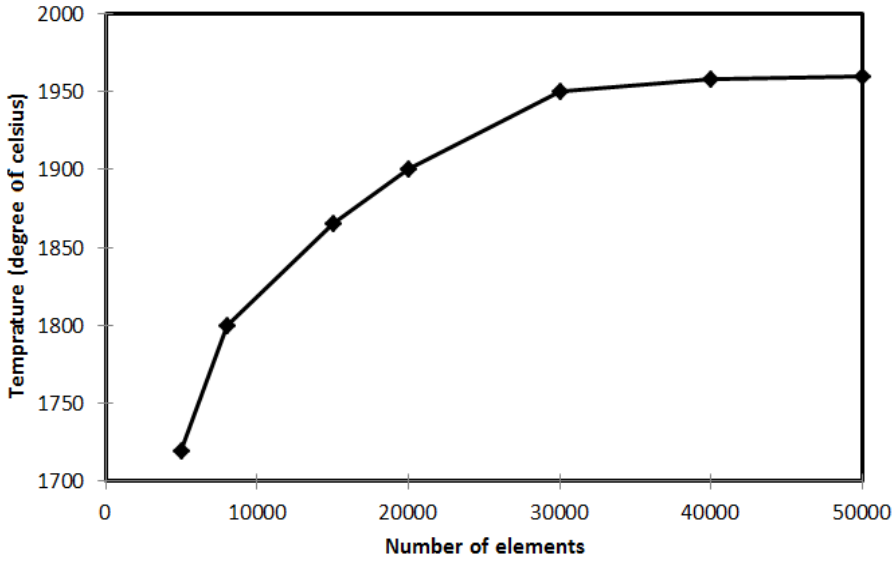

Figure 4 Variation of meshes compare to maximum temperature in the center of the weld region versus the number of elements

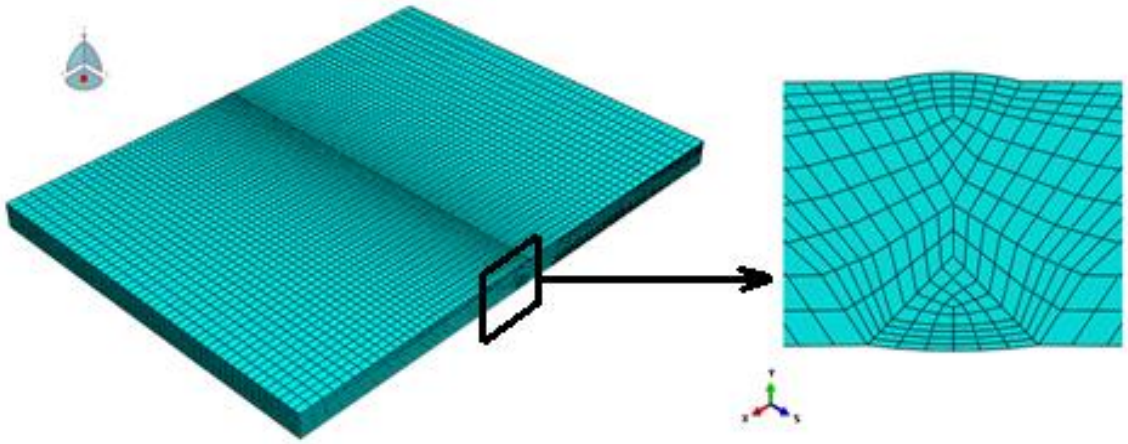

Figure 5 FE meshes for the weld region of the sample

4.1 HT discretization

During the HT, the pipe withstands a specified internal pressure. According to the American water work association (AWWA) [36], the pressure of the HT can be calculated from the following equation:

$$P = \left(\frac{2\sigma_H t}{D_0}\right) = K\left(\frac{2\sigma_y t}{D_0}\right) \quad (9)$$

P (MPa) is the minimum pressure for HT. *K* is the ratio of hoop stress generated by the HT to the minimum yield strength of the material ($\frac{\sigma_H}{\sigma_y}$). D_0 is the outside diameter of the pipe and *t* is its thickness. According to IPS suggestion, the minimum number for *K* is 0.95 [37]. Hoop stress in a simple pipe is calculated as 239MPa with a hydrostatic pressure of 5.6 MPa. Longitudinal strain is zero during the HT. A finite length of pipe is simulated and longitudinal stress (σ_L) is found 70MPa.

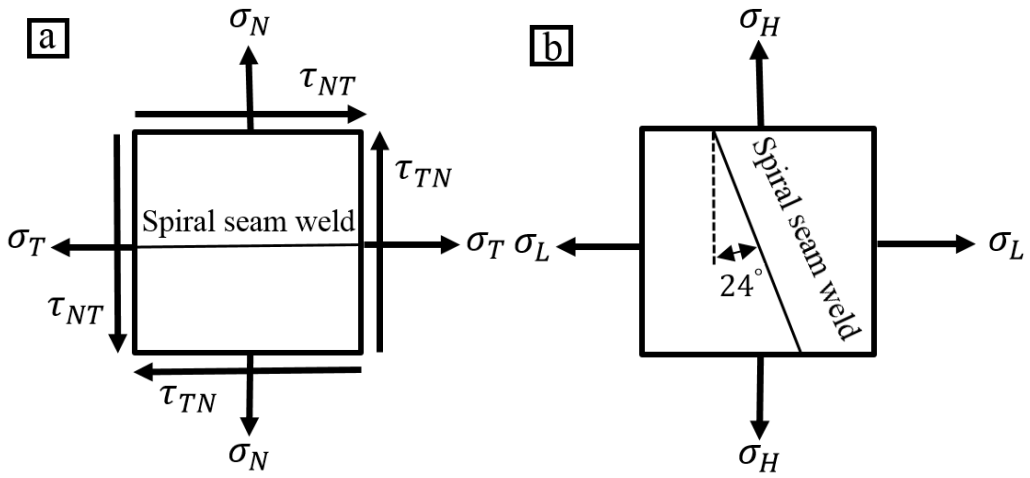

a- Stress distribution on the sample

b- longitudinal and circumference RS

Figure 6 Stress distribution on the sample

Stresses in the spiral WS are shown in figure (6), σ_L and σ_H are not perpendicular and parallel to the WS direction respectively. Therefore, using stress transformation equations σ_T , σ_N and τ_{NT} are considered.

Stress transformation equations are as follows:

$$\begin{aligned}\sigma_T &= \sigma_H \cos^2\theta + \sigma_L \sin^2\theta + \tau_{LH} \sin 2\theta \\ \sigma_N &= \sigma_H \sin^2\theta + \sigma_L \cos^2\theta - \tau_{LH} \sin 2\theta \\ \tau_{TN} &= \tau_{LH} \cos 2\theta - \frac{\sigma_L + \sigma_H}{2} \sin 2\theta\end{aligned} \tag{10}$$

Where $\theta = -24, \sigma_T = 209.7\text{MPa}, \sigma_N = 141.8\text{MPa}$ and $\tau_{SH} = \sigma_S = 0$. This loading condition was exerted on the sample in two different steps. In the first step, the internal pressure is linearly increased from zero to 5.6 MPa, then in the next step, this pressure is linearly decreased to zero.

4.2 Validation of the results

Table (3) compares the tangential RS values on the external side of the sample before the HT obtained through experimental tests and FE simulation.

Table 3 Comparison of tangential RS on the external side of the sample before the HT

Number of strain rosette	Distance from the WS (mm)	Experimental RS (MPa) [4]	RS calculated by the FE (MPa)	Percent of Error	FE of RS (MPa) [4]	Percent of Error
1	10	340	420	24	400	15
2	20	430	450	5	425	1
3	30	350	300	14	260	26
4	40	305	250	18	225	26
5	50	205	200	2	200	2
6	60	150	170	13	140	7

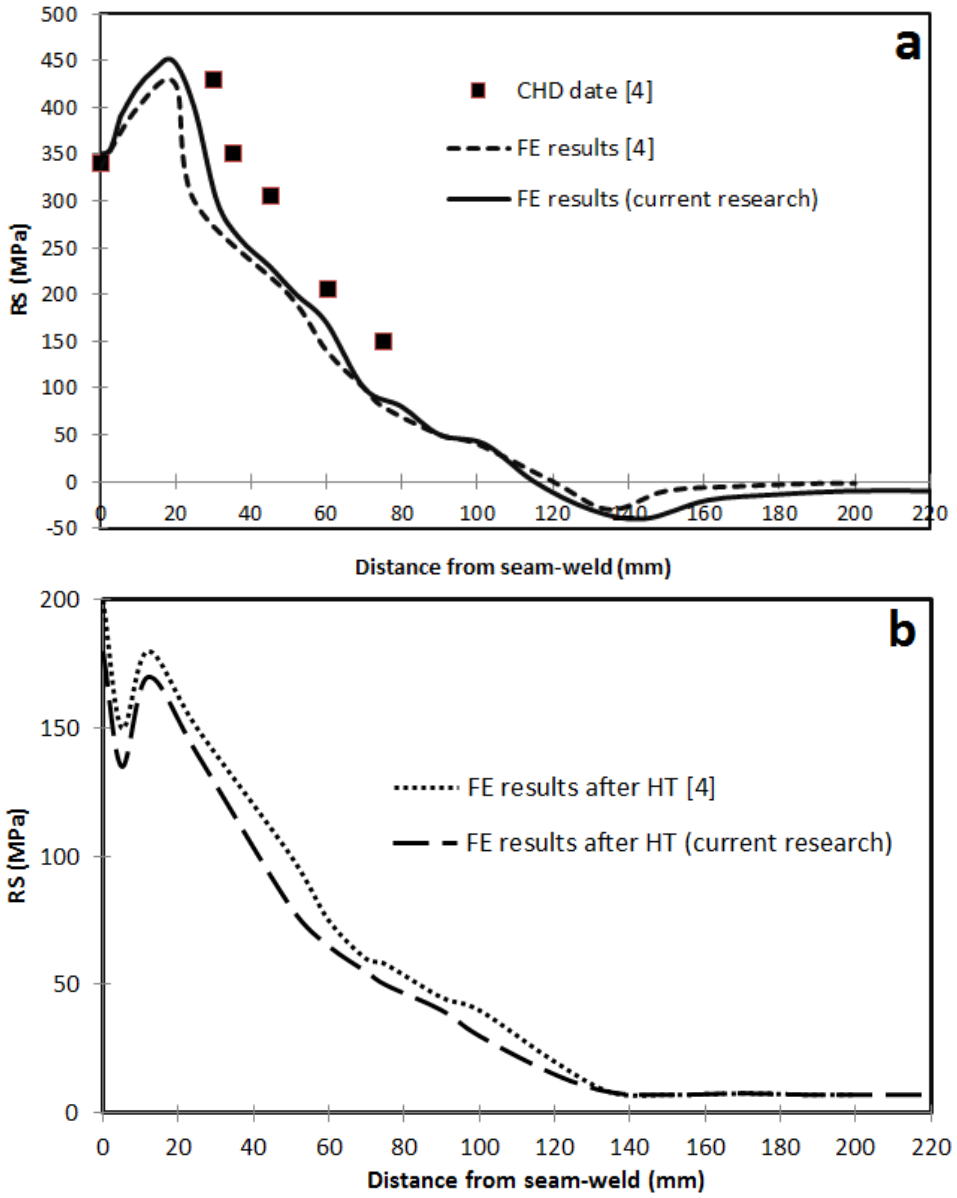

Figure 7 Tangential RS on the external side of the sample for API-X70 steel (**a**: prior to HT **b**: after HT)

Employing a trial and error approach dimension of 320×440 mm was seen suitable for API-X70 steel. Figure (7) shows Tangential RS on the external side of the sample. Results are in agreement with the results of reference [4]. Comparison between tangential RS obtained through experimental tests and the RS calculated by FE on the external side of the model prior to the HT is also shown in table (3).

5 Experimental mensuration

Schajer has done various investigations of CHD principles and introduced extensive advancements to determine RS by CHD [37, 38, 39]. Measurements were brought out on the chosen sample from a hydrostatically tested pipe. Therefore, in this work, the CHD method was used to determine the RS. First of all, strain gauge rosettes were mounted on the internal and external sides of the sample.

Then, RS values were measured in six points on the external and internal sides of the sample. The location of rosettes on both sides of the sample is shown schematically in figure (9a). Installed rosettes on the external sides of the sample are shown in figure (9b); the same rosette positions were installed on the internal surface. All rosettes consist of three strain gages; two of them are orthogonal and normal to the WS. The drilling has been done carefully; data were recorded in 10 steps with 0.2 mm drilling depth increments each time. Moreover, the diameter of the drill was 1.82 mm which rotates quite fast by a motor speed of 300,000 rpm. This high speed is required to avoid strain hardening of the material located near the hole. The apparatus used to do CHD measurement is shown in figure (9c). The detailed principles of CHD are published [22]. CHD, measurements, and calculations were conducted according to the ASTM E837 Standard [21].
Although a likewise experience had been done in the work of ref [4], there is an important and determining difference in comparison with our study. The weld cap in the former has been initially removed to install the rosettes on a flat surface. However, in our test, the rosettes were installed without eliminating the weld cap, because removing weld caps could change the value of residual stress in the weld metal region. Therefore, experimental results obtained by the CHD technique are more accurate in the present study. Thus, the rosettes were mounted next to the weld cap in the positions shown in figure (8).

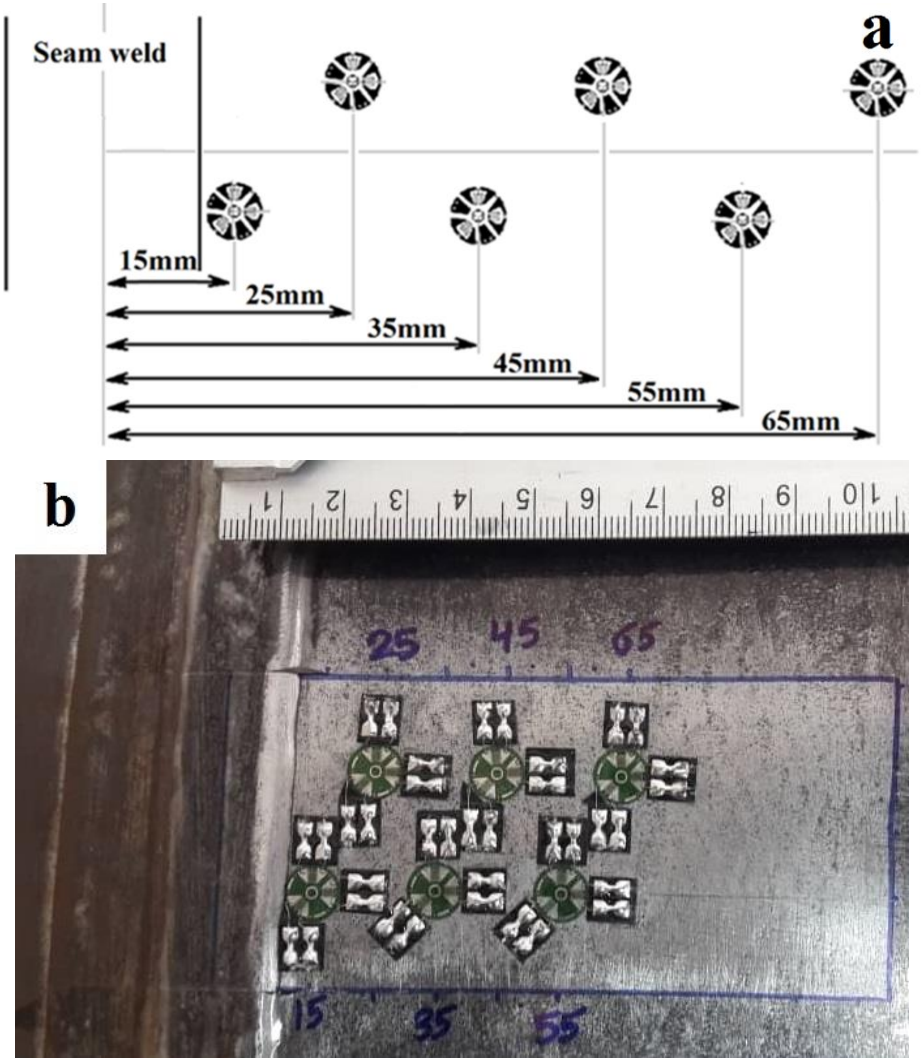

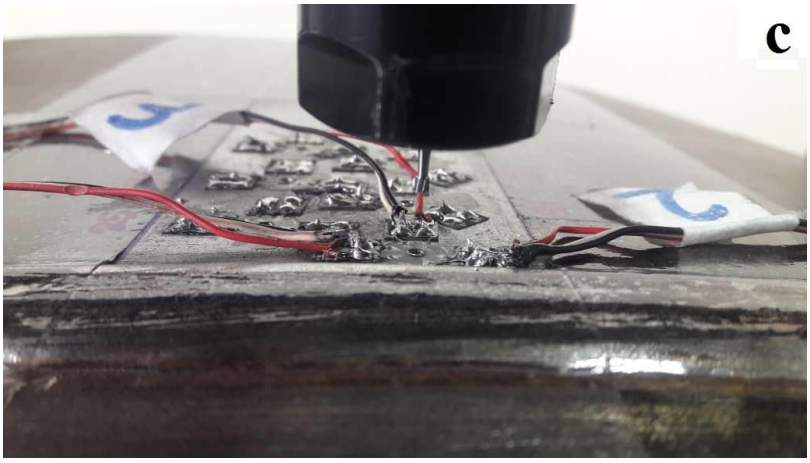

Figure 8 (**a**) Location of rosettes on the internal and the external sides of the sample; (b): rosettes bounded on the external side of the sample; (c) CHD Piercing apparatus

6 Results and discussions

Simulation of API-X65 is done based on the related parameters in terms of heat transfer and stress analysis [30]. Results are discussed as follows:

6.1 RS on the external side of the sample

Tables (4) and (5) compare the tangential and normal RS on the external side of the sample after HT respectively. Tangential RS (σ_T) on the external side of the sample is reported in figure (10). From the WS to 102 mm distance from WS, tangential RS is tensile, and after that, as the distance increases the RS becomes compressive and finally approaches zero.

Table 4 Comparison of tangential RS on the external side of the sample after HT

Number of strain rosette	Distance from the WS (mm)	Experimental RS (MPa)	RS calculated by the FE (MPa)	Percent of Error
1	15	318	243	24
2	25	291	170	42
3	35	95	132	40
4	45	69	75	9
5	55	97	65	33
6	65	33	50	51

Table 5 Comparison of normal RS on the external side of the sample after HT

Number of strain rosette	Distance from the WS (mm)	Experimental RS (MPa)	RS calculated by the FE (MPa)	Percent of Error
1	15	-167	-108	35
2	25	-45	-55	22
3	35	-28	-9	68
4	45	1	1.5	50
5	55	46	57.5	25
6	65	66	40	40

Normal RS (σ_N) on the external side of the sample is demonstrated in figure (10). Normal RS is compressive from the WS to the distance of 40 mm from that and after that RS becomes tensile. RS is compressive in the HAZ because of the self-equilibrium manner of RS. HAZ has a twosome manner because the material which doesn't melt gets doughy so it has the same manner as WM. Furthermore, because of the high-temperature gradient, the microstructure of HAZ is course-grained martensite so a transmission behavior between WM and base-metal is rational. Differences between FE and CHD results are because of not only the variation of RS in the thickness direction but also the modeling of the sample as a flat plate.

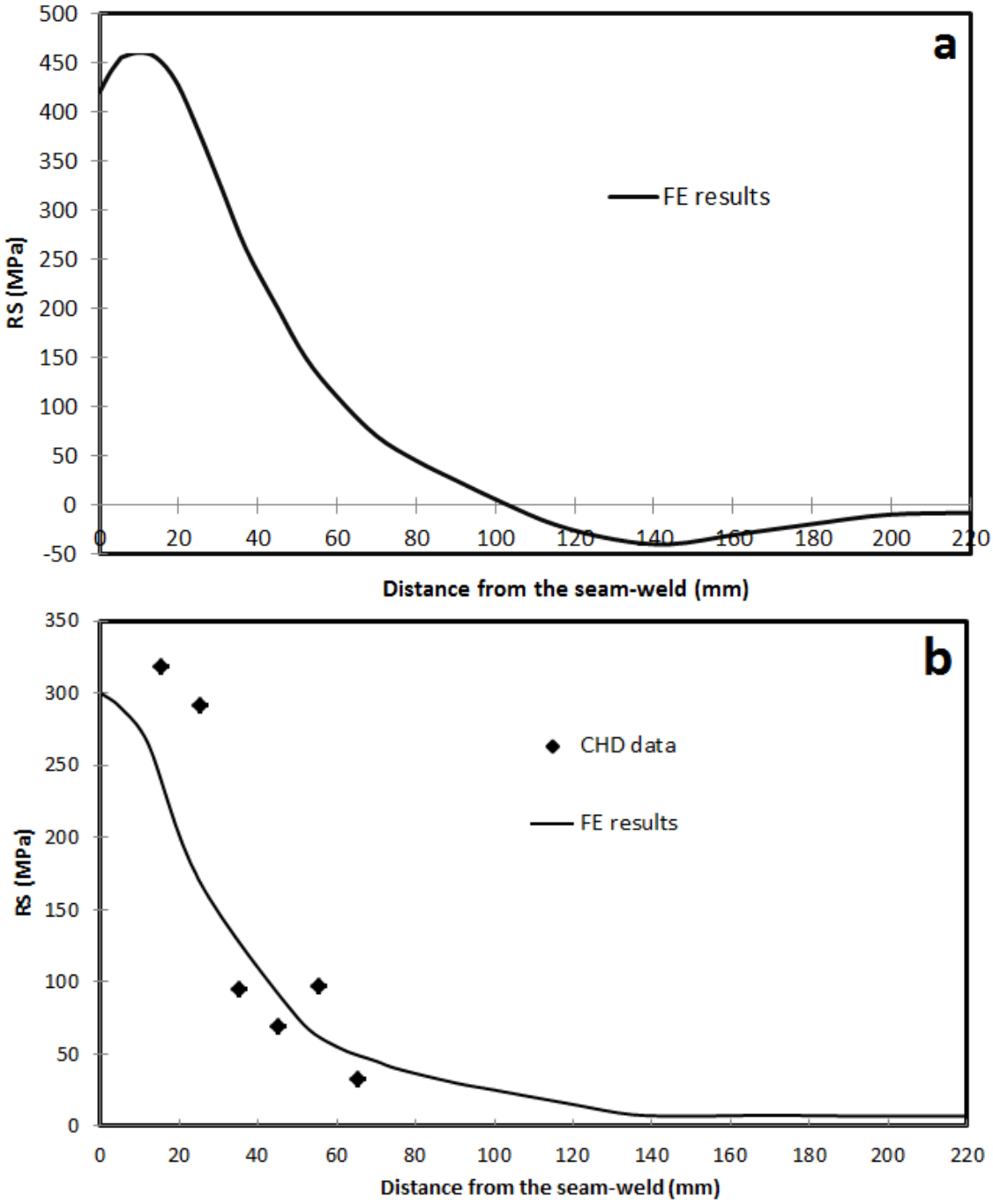

Figure 9 Tangential RS on the external side of the sample (**a**: before HT **b**: after HT)

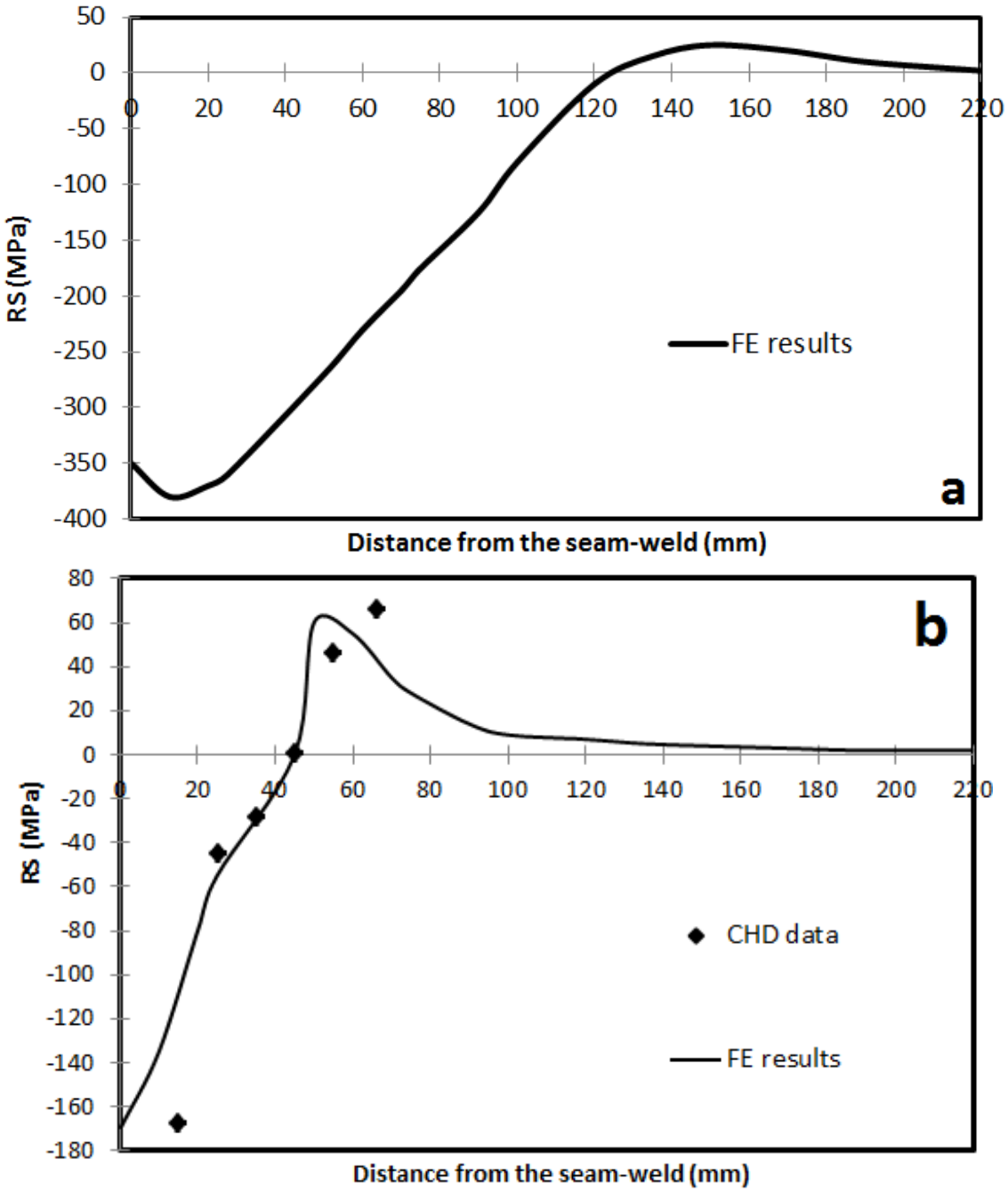

Figure 10 Normal RS on the external side of the sample (**a**: before to HT **b**: after HT)

Table (6) shows the RS state on the external side of the sample (MPa).

Table 6 RS state on the external side of the sample (MPa)

RS	RS after HT		RS after welding process		Distance from the WS (mm)	
	Normal	Tangential	Normal	Tangential	Normal	Tangential
Maximum RS	-170	300	-379	455	-	15
RS in the WS	-170	300	-351	423	-	-

6.2 RS on the internal side of the sample

Tables (7) and (8) compare the tangential and normal RS on the internal side of the sample after the HT respectively. Tangential RS (σ_T) on the external side of the sample is presented in figure (11). After the welding procedure, tangential RS is tensile from the WS to the distance of 114 mm from the WS, and after that RS will become compressive and finally approach zero.
Normal RS (σ_N) on the external side of the sample is demonstrated in figure (12). After the welding procedure, normal RS is compressive from the WS to the distance of 40 mm from that, and after that RS will become tensile. Differences between the results of CHD and FE can be caused by the spiral rolling of the plate in the production process of the pipe. Furthermore, the electrical current of welding, geometry of the WS, martensite microstructure, diameter of the welding torch, welding travel speed, and stresses created in the production process are other affecting factors. Table (6) depicts RS on the external sides of the sample. Tables (7) and (8) compare tangential and normal RS on the external sides of the sample.

Table 7 Comparison of tangential RS on the internal side of the sample after the HT

Number of strain rosette	Distance from the WS (mm)	Experimental RS (MPa) [4]	RS calculated by the FE (MPa)	Percent of Error
1	15	380	322	15
2	25	344	296	14
3	35	221	281	27
4	45	272	234	14
5	55	248	202	19
6	65	225	159	30

Table 8 Comparison of normal RS on the internal side of the sample after the HT

Number of strain rosette	Distance from the WS (mm)	Experimental RS (MPa) [4]	RS calculated by the FE (MPa)	Percent of Error
1	15	-103	-33	68
2	25	6	10	67
3	35	126	57	55
4	45	192	184	4
5	55	177	161	9
6	65	147	102	31

Table 9 RS state on the internal side of the sample (MPa)

RS	RS after HT		RS after welding process		Distance from the WS (mm)	
	Normal	Tangential	Normal	Tangential	Normal	Tangential
Maximum RS	-106	350	-287	498	-	13
RS in the WS	-106	350	-287	450	-	-

Table (9) shows the RS state on the internal side of the sample.

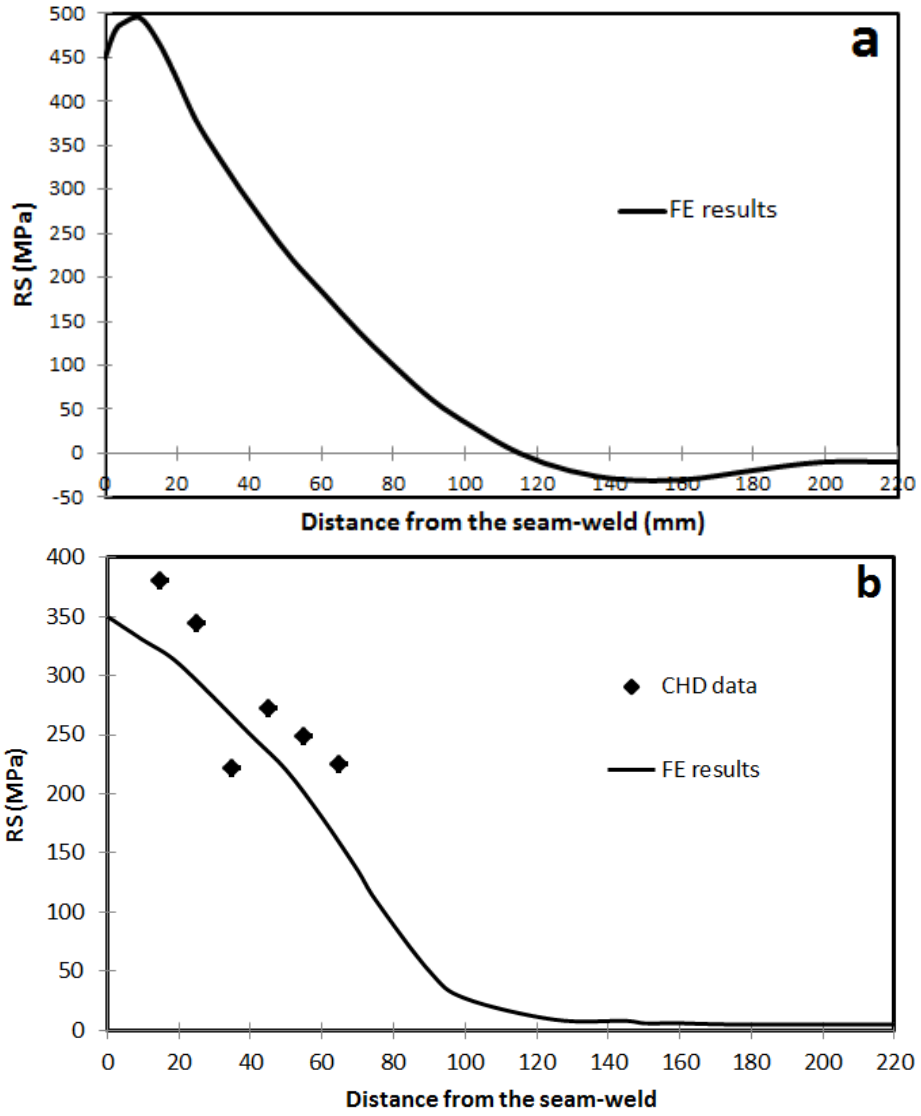

Figure 11 Tangential RS on the internal side of the sample (**a**: before HT **b**: after HT)

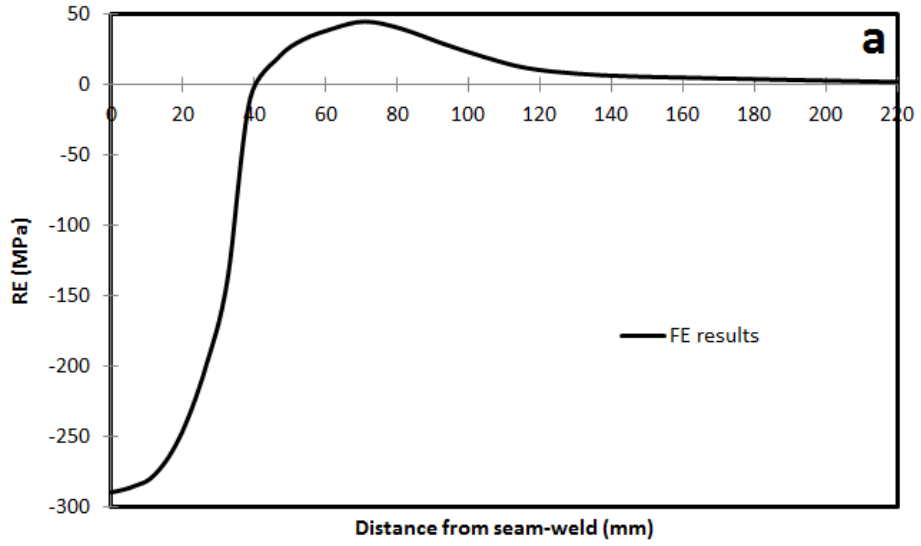

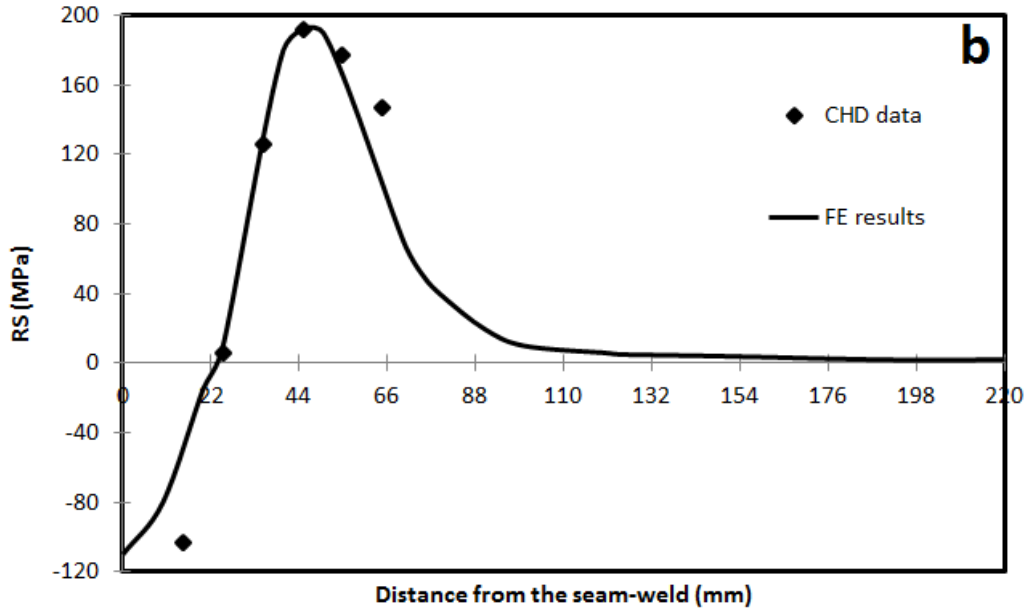

Figure 12 Normal RS on the internal side of the sample (**a**: before HT **b**: after HT)

6.3 RS in the thickness direction

RS on each side of the specimen can be determined by the CHD technique. However, the CHD technique is not able to find RS in the direction of thickness. Moreover, the intensity of changes of RS in the direction of thickness is important, because the validation of the CHD technique depends on it [1]. However, if the wall thickness of the pipe would be thin enough, RS become negligible in the thickness direction. As well as, external passes of the welding procedure decrease RS caused by internal passes like a heat-treatment process. Furthermore, RS is asymmetric in the direction of thickness due to different arrangements of the welding passes.
Von Mises RS is determined by the following equation:

$$\sigma_e^2 = \sigma_T^2 + \sigma_N^2 - \sigma_T\sigma_N + 3\tau_{NT}^2 \tag{11}$$

Figure (13) shows Von Mises residual stress in direction of the thickness measured in the WS. Accordingly, the maximum values of RS are reported on the sides of the specimen. In addition, the minimum value of RS is decreased from 220 MPa to 140 MPa after the HT (36% reduction), and the maximum value of RS is decreased from 460 MPa to 270 MPa after the HT (41% reduction). The measurement of the residual stress in the thickness direction is unprecedented, although it is contributing to know while performing CHD technique. The greater the variation of residual stress values in this direction, the more incorrect would be the results of CHD. Therefore, it is determining to make sure that this variation is not considered before the CHD technique. If the residual stress values in this direction are different, the results of CHD would probably be deviated from what is obtained from the FE simulation. In other words, this variation can be expressed as a possible cause to explain the differences between theoretical and experimental results.
Figure (14a) and (14b) show tangential and normal RS in the direction of thickness in WS. The maximum values of RS are reported on the surfaces of the specimen. In the middle of wall thickness at the WS, RS decreases in a way that would satisfy the equilibrium of stresses. It is also evident that critical values of residual stresses are located in the HAZ.

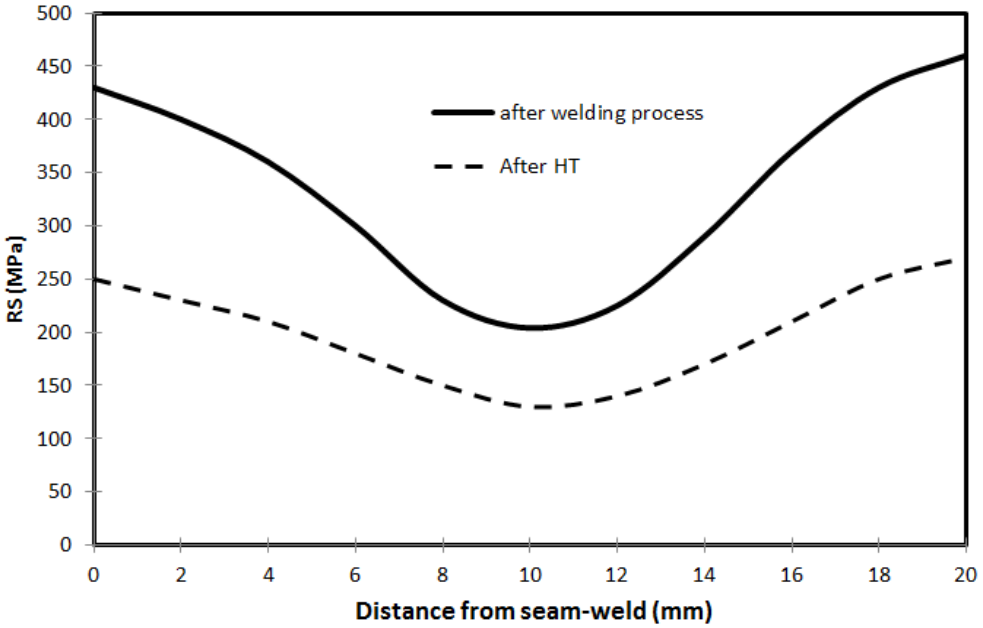

Figure 13 Von Mises RS in the thickness direction for the FE model

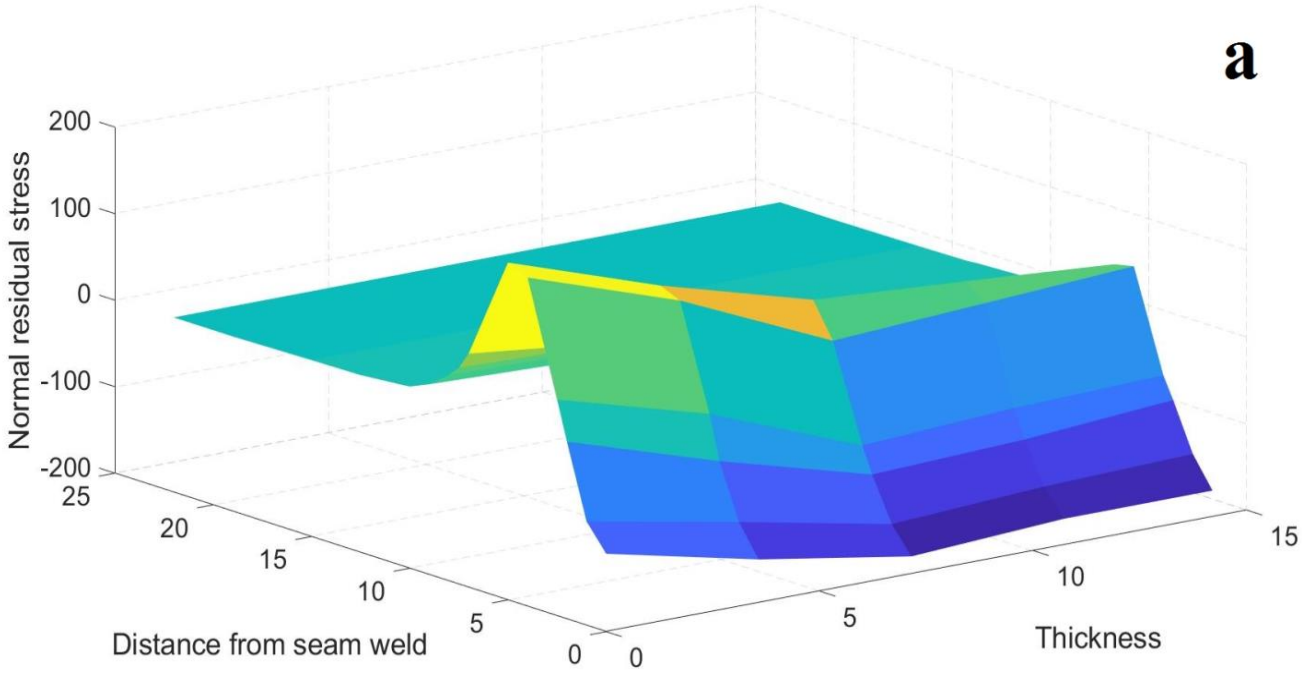

7 Results and discussion

According to reference [4], a sample with the dimensions of 320×440 mm was predicted convenient, then simulation of the welding process was done on it. Results are validated considering their close accordance with the results of reference [4]. Thus, this portable standard sample can be used instead of the main pipe to do the CHD test. Maximum normal stress is reported

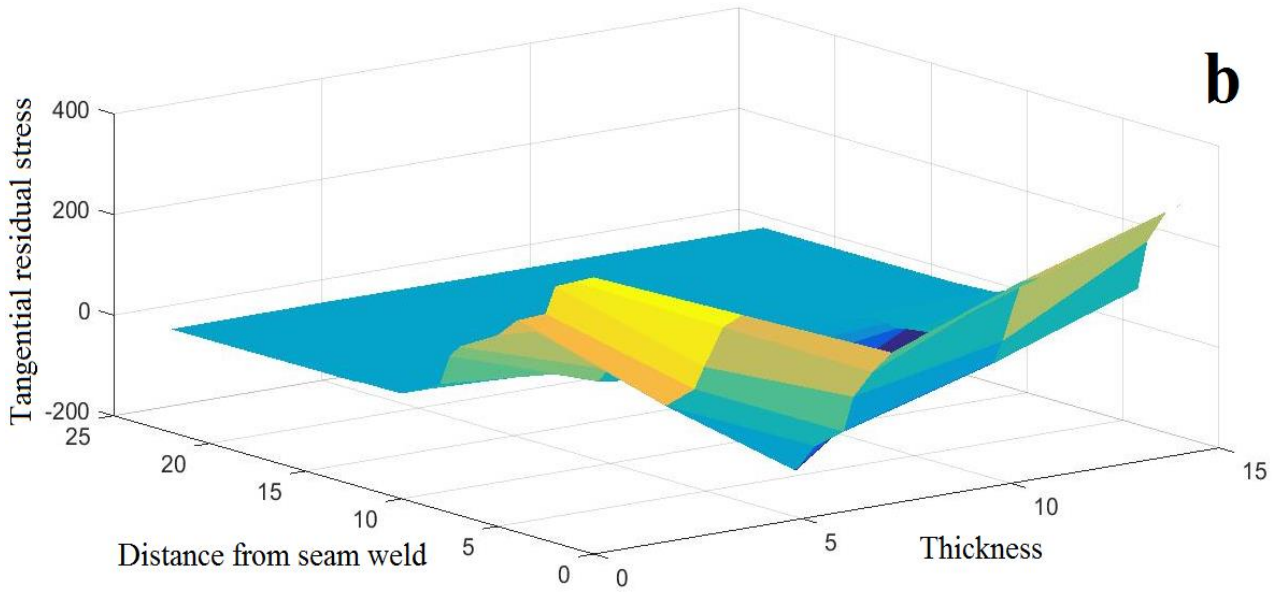

Figure 14 RS in the direction of the thickness (**a**: tangential **b**: normal HT)

in the HAZ and this stress decreases to zero far from there in the base metal. Tangential RS is of the maximum value in the vicinity of WS and decreases to zero far from there. The yield strength of API-X65 is 500 MPa in the ambient temperature. Moreover, the residual stress is more than half of the yield strength of the material in the HAZ. Therefore, there are some errors in the results achieved by applying CHD in these regions. Tangential RS has maximum errors of 34% on the external side of the specimen. Stress changes in the direction of thickness are reported in this study for the first time and it is important because of validation of the CHD technique. It is proved that the maximum value of RS in the thickness direction is certainly located on the pipe sides. HT decreases RS in the thickness direction and its minimum value is located in the middle of the thickness of the pipe wall and it is compressive.

The following results are reported:

1- The total area above and below tangential and normal stress curves is not generally equal, as a result, the equilibrium of stresses should be satisfied in the thickness direction. This fact is a poof for the importance of residual stresses in the thickness direction.

2- The validity of results is supported by results of reference [4].

3- High tangential RS is reported in the HAZ and RS decreases far from WS and it is because of the high-temperature gradient in the welding region.

4- High normal RS values are reported in the HAZ and RS values increase far from WS.

5- Far from WS, normal and tangential stresses are relatively constant.

6- Before the HT because RS is higher than half of the yield strength of the material, error in the results of CHD should be considered.

7- Maximum tangential and normal RS on the external side of the sample is decreased by 68% in the WS and HAZ.

8- The total area above and below tangential and normal stress curves is not generally equal, as a result equilibrium of stresses should be satisfied in the thickness direction. This fact is a poof for importance of residual stresses in the thickness direction.

9- Thermal process of welding filler pass decreases RS distribution in the welding root pass.

Because the results of a finite sample used in the work presented in this paper are consistent with reference [4], this finite sample can be used instead of a heavy and unwieldy pipe which is quite

helpful in saving time, energy, and money. Moreover, considering the variation in the values of RS in the thickness direction is vitally important, especially in determining the reliability of CHD results. It would be a necessity to investigate how the variation would influence the CHD results.

8 Conclusion

It was proved that the separation of a finite and portable sample from the main pipe is both convenient and yields acceptable results. CHD tests were done on an intact sample containing weld cap, consequently, the results are more accurate than previous studies eliminating weld cap. Moreover, residual stresses in the thickness direction have been clarified for the first time. Through thickness residual stresses are vitally important because validation of CHD results are directly related to them; the more intense the stress variation, the more inexact the experimental results become. The effect of the curvature of the sample could be taken into account in future works.

Acknowledgments

The authors wish to thank Dr. M. Forouzan for the support of this research, and Dr. R. Moharrami from the residual stress laboratory of Zanjan University for performing the experimental measurements.

Data Availability Statement

Validation datasets for this research are included in Forouzan, M., et al. (2012) at [10.1016/j.matdes.2011.04.016].

References

[1] Schajer, G., "*Residual Stresses: Measurement by Destructive Testing*", Encyclopedia of Materials: Science and Technology, ISBN: 978-0-08-043152-9, University of British Columbia, Vancouver, British Columbia, Canada, pp. 8152-8158, (2011).

[2] Majzoobi, G.H., Seifi, R., and Ali-akbar, S., "Experimental and Numerical Study of Temperature Distribution and Determination of Residual Stresses due to Welding of Plates", Journal of Modeling in Engineering, Vol. 9, No. 27, pp. 49-60, (2012).

[3] Sattari-Far, I.a., and Farahani, M., "Effect of the Weld Groove Shape and Pass Number on Residual Stresses in Butt-welded Pipes", International Journal of Pressure Vessels and Piping, Vol. 86(11), pp. 723-731, (2009).

[4] Forouzan, M., Mirfalah Nasiri, S.M., Mokhtari, A., and Heidari, A., "Residual Stress Prediction in Submerged Arc Welded Spiral Pipes", Materials and Design, Vol. 33, pp. 384-394, (2012).

[5] Habibi, N., Hassani-Gangaraj, S.M., Farrahi, G.H., Majzoobi, G.H., Mahmoudi, A.H., Mahmoudi, A., Yari-Brojeni, A., Moridi, A., and Daghigh, M., "The Effect of Shot Peening on Fatigue Life of Welded Tubular Joint in Offshore Structure", Materials and Design, Vol. 36, pp. 257-250, (2012).

[6] Farrahi, G.H., Majzoobi, G.H., Mahmoudi, A.H., and Habibi, N., "Fatigue Life of Repaired Welded Tubular Joints", International Journal of Engineering, Vol. 26, pp. 31-25, (2013).

[7] Habibi, N., and Eskandari, H., "Stress and Temperature Analysis in Tubular X-joints using Simufact Welding", Journal of Welding Science and Technology (JWSTI), Vol. 5(2), pp. 61-75, (2020).

[8] Nobre, J., Polese, C., and Staden, S., "Incremental Hole Drilling Residual Stress Measurement in Thin Aluminum Alloy Plates Subjected to Laser Shock Peening", Experimental Mechanics, Vol. 60(1), pp. 1-12, (2020).

[9] Nakhodchi, S., Akbari Iraj, S., Shokuhfar, A., and Rezazadeh, H., "Numerical and Experimental Study of Temperature and Residual Stress in Multi-pass Welding of Two Stainless Steel Plates Having Different Thicknesses", Modares Mechanical Engineering (MME), Vol. 14(9), pp. 81-9, (2014).

[10] Sabokrouh, M., Hashemi, S.H., and Farahani, M.R., "Experimental Determination of Residual Stresses in Multi-pass Girth Welding of Thermo-mechanical Steel Pipe", Journal of Applied and Computational Sciences in Mechanics (Journal of School of Engineering) (JACM), Vol. 25, pp. 111-120, (2013).

[11] Charkhi, M., and Akbari, D., "Application of Pre-heating in the Reduction of Residual Stress in the Repair Welds of Steel Pipes", Modares Mechanical Engineering (MME), Vol. 17, pp. 1-10, (2018).

[12] Shiri, A., and Heidari, A., "Investigating the Effect of Joint Geometry of the Gas Tungsten Arc Welding Process on the Residual Stress and Distortion using the Finite Element Method", Journal of Solid Mechanics, Vol. 11(4), pp. 736-746, (2019).

[13] Qiang, B., Li, Y., Yao, C., and Wang, X., "Through-thickness Welding Residual Stress and its Effect on Stress Intensity Factors for Semi-elliptical Surface Cracks in a Butt-welded Steel Plate", Engineering Fracture Mechanics, Vol. 193, pp. 17-31, (2018).

[14] Xin, H., and Veljkovic, M., "Residual Stress Effects on Fatigue Crack Growth Rate of Mild Steel S355 Exposed to Air and Seawater Environments", Materials and Design, Vol. 193, Article Number: 108732, https://doi.org/10.1016/j.matdes.2020.108732, (2020).

[15] Wan, Y., Jiang, W., Song, M., Huang, Y., Li, J., Sun, G., Shi, Y., Shai, X., Zhao, X., and Ren, L., "Distribution and Formation Mechanism of Residual Stress in Duplex Stainless Steel Weld Joint by Neutron Diffraction and Electron Backscatter Diffraction", Materials and Design, Vol. 181, Article Number: 108086, https://doi.org/10.1016/j.matdes.2019.108086, (2019).

[16] Goel, S., Neikter, M., Capek, J., Polatidis, E., Colliander, M.H., Joshi, S., and Pederson, R., "Residual Stress Determination by Neutron Diffraction in Powder Bed Fusion-built Alloy 718: Influence of Process Parameters and Post-treatment", Materials and Design, Vol. 195, Article Number: 109045, https://doi.org/10.1016/j.matdes.2020.109045, (2020).

[17] Ma, W., Zhang, H., Zhu, W., and Xu, F., "Study on Residual Stress of Welded Hoop Structure", Applied Sciences, Vol. 10(8), Article Number: 2838, DOI:10.3390/app10082838 (2020).

[18] Magnier, A., Zinn, W., Niendorf, T., and Scholtes, B., "Residual Stress Analysis on Thin Metal Sheets using the Incremental Hole Drilling Method–fundamentals and Validation", Experimental Techniques, Vol. 43(1), pp. 65-79, (2019).

[19] Beghini, M., Bertini, L., and Giri, A., "Measuring Residual Stress in Finite Thickness Plates using the Hole-drilling Method", The Journal of Strain Analysis for Engineering Design, Vol. 54(1), pp. 65-75, (2019).

[20] Yan, X., and Yang, C., "Experimental Research and Analysis on Residual Stress Distribution of Circular Steel Tubes with Different Processing Techniques", Thin-Walled Structures, Vol. 144, Article Number: 106268, https://doi.org/10.1016/j.tws.2019.106268 (2019).

[21] Hashemi, S., and Mohammadyani, D., "Characterisation of Weldment Hardness, Impact Energy and Microstructure in API X65 Steel", International Journal of Pressure Vessels and Piping, Vol. 98, pp. 8-15, (2012).

[22] Rajabi, M., and Hashemi, S., "Numerical Simulation of Submerged Spiral Arc Welding on API X70 Gas Transmission Steel Pipe", Modares Mechanical Engineering, Vol. 20(3), pp. 739-750, (2020).

[23] Hibbitt, H.D., Karlsson, B.I., and Sorensen, E.P., "ABAQUS/Standard: User's Manual", Hibbitt, Karlsson and Sorensen, Vol. 1, (1997).

[24] Michaleris, P., and Debiccari, A., "Prediction of Welding Distortion", Welding Journal-Including Welding Research Supplement, Vol. 76(4), pp. 172-181, (1997).

[25] Fricke, S., Keim, E., and Schmidt, J., "Numerical Determination of Residual Weld Stresses", Proceedings of ICES (Proceedings, ICES'98), Vol. 98, pp. 7-9, Atlanta, USA, (1998).

[26] Dong, Y., Hong, J.K., Tsai, C.L., and Dong, P., "Finite Element Modelling of Residual Stresses in Austenitic Steel Pie Girth Welds", Welding Journal-Including Welding Research Supplement , Vol. 76(10), pp. 442-449, (1997).

[27] Zhang, J., and Dong, P., "*3-D Residual Stress Charactristics in Pipe Repair Welds*", Trends in Welding Research: Proceedings of the 5th International Conference, Pine Mountain, Georgia, USA, June 1 - 5, 1. print (English), (1998).

[28] Deshpande, A., Tanner, D., Sun, W., Hyde, T., and McCartney, G., "Combined Butt Joint Welding and Post Weld Heat Treatment Simulation using SYSWELD and ABAQUS", Proceedings of the Institution of Mechanical Engineers, Part L: Journal of Materials: Design and Applications, Vol. 225(1), pp. 1-10, (2011).

[29] Withers, P.J., and Bhadeshia, H.K.D.H., "Residual Stress. Part 1 – Measurement Techniques", Materials Science and Technology, Vol. 17(4), pp. 355-365, (2001).

[30] Goldman, T., "New Joining Technology for Metal Pipe in the Construction Industry", Break-through Strategy Committee, Texas, pp. 1-25, (2003).

[31] Nezamdost, M., Nekouie Esfahani, M.R., Hashemi, S.H., and Mirbozorgi, S.A., "Investigation of Temperature and Residual Stresses Field of Submerged Arc Welding by Finite Element Method and Experiments", The International Journal of Advanced Manufacturing Technology, Vol. 87(1-4), pp. 615-624, (2016).

[32] Huang, X., Liu, Z., and Xie, H., "Recent Progress in Residual Stress Measurement Techniques", Acta Mechanica Solida Sinica, Vol. 26(6), pp. 570-583, (2013).

[33] Goldak, J., Chakravarti, A., and Bibby, M., "A New Finite Element Model for Welding Heat Sources", Metallurgical Transactions B, Vol. 15(2), pp. 299-305, (1984).

[34] Sedighi, M., and Nazemnezhad, R., "Effect of Peak Positioning Method on Accuracy of X-ray Diffraction Residual Stress Measurement", Experimental Techniques, Vol. 40(1), pp. 295-302, (2016).

[35] Masoumi, M., Herculano, L.F.G., and Abreu, H.F.G., "Study of Texture and Microstructure Evaluation of Steel API 5L X70 under Various Thermomechanical Cycles", Materials Science and Engineering: A, Vol. 639, pp. 550-558, (2015).

[36] Arnaout, S., Slavin, L., "*Pipelines 2013: Pipelines and Trenchless Construction and Renewals—A Global Perspectiv*e", ISBN (print): 9780784413012, American Society of Civil Engineers (ASCE), June 23-26, Fort Worth, Texas, United States, pp. 398-410, (2013).

[37] Schajer, G.S., "Advances in Hole-drilling Residual Stress Measurements", Experimental Mechanics, Vol. 50(2), pp. 159-168, (2010).

[38] Schajer, G.S., Winiarski, B., and Withers, P., "Hole-drilling Residual Stress Measurement with Aartifact Correction using Full-field DIC", Experimental Mechanics, Vol. 53(2), pp. 255-265, (2013).

[39] Schajer, G.S., "Hole-drilling Residual Stress Measurements at 75: Origins, Advances, Opportunities", Experimental Mechanics, Vol. 50(2), pp. 245-253, (2010).

Nomenclatures

a.b.c	Sections of heat source
C	Goldak constant
D	Diameter (mm)
f_f	The thermal parameter in the front of Goldak model
f_r	The thermal parameter in the back of Goldak model
H	Convection coefficient ($Wm^{-2}{}^{o}C^{-1}$)

CHD	Central hole drilling
HT	Hydrostatic test
h_C	Convection coefficient ($Wm^{-2}{}^oC^{-1}$)
h_r	Radiation coefficient ($Wm^{-2}{}^oC^{-1}$)
I	Electrical current (A)
K	The ratio of hoop stress of HT to yield strength of the material, conduction coefficient
P	Pressure of HT (MPa)
Q	Thermal heat flux (Wm^{-2})
T	Thickness (mm)
V	The voltage of welding arc (V), coefficient of kinematic viscosity, welding speed

Abbreviations

AWWA	American water work association
CHD	Central hole drilling
FE	Finite element simulation
GTAW	Gas tungsten arc welding
HAZ	Heat affected zone
HT	Hydrostatic test
RS	Residual stress
SAW	Submerged are welding
SMAW	Shielded metal are welding
TIG	Tungsten inert gas
WS	Weld seam
WM	Weld metal region

Greek Symbols

A	Angle to the loading direction
φ	Spiral angel
θ	Temperature (°C)
σ	RS (MPa)
σ_e	Von Mises stress
σ_L	longitudinal stress
σ_H	hoop stress
σ_N	normal stress to the WS
σ_T	tangential stress to the WS
τ	Shear stress exerted on the sample
η	The efficiency of the electrical arc

Captions

eq	Equal
G	Center of the portable coordinate
O	Outer